Non-periodic motions and fractals of a circular arch under follower forces with small disturbances

Nobuyoshi Fukuchi[†]

Graduate School of Engineering, Kyushu University, 6-10-1, Hakozaki, Higashi-ku,
Fukuoka 812-8185, Japan

Takashi Tanaka[‡]

Japan Marine Science Inc., 2-3-6 Minami-Shinagawa, Shinagawa-ku, Tokyo 140-0004, Japan

Abstract.   The deformation and dynamic behavior mechanism of submerged shell-like lattice structures with membranes are in principle of a non-conservative nature as circulatory system under hydrostatic pressure and disturbance forces of various types, existing in a marine environment. This paper deals with a characteristic analysis on quasi-periodic and chaotic behavior of a circular arch under follower forces with small disturbances. The stability region chart of the disturbed equilibrium in an excitation field was calculated numerically. Then, the periodic and chaotic behaviors of a circular arch were investigated by executing the time histories of motion, power spectrum, phase plane portraits and the *Poincare* section. According to the results of these studies, the state of a dynamic aspect scenario of a circular arch could be shifted from one of quasi-oscillatory motion to one of chaotic motion. Moreover, the correlation dimension of fractal dynamics was calculated corresponding to stochastic behaviors of a circular arch. This research indicates the possibility of making use of the correlation dimension as a stability index.

Keywords: dynamic stability; non-conservative nature; circular arch; follower force; instability region; correlation dimension; chaotic behaviors.

1. Introduction

The development of marine resources and the utilization of marine space have shown progress in recent years. The homeo-thermal property of an underwater environment is especially useful for stocking provisions, such as a surplus of agricultural produce in a year of good harvest. To fulfill this purpose, a structure is needed which is both large-scale and constructed of comparatively flexible material for reasons of cost efficiency. One structure which satisfies these conditions is a shell-like structure composed of circular arches and membranes, provided that it can protect the underwater loads from downward hydrostatic pressure.

The deformation and dynamic behavior mechanisms of submerged shell-like lattice structures

---

†Professor, Corresponding author, E-mail: fukuchi@nams.kushu-u.ac.jp
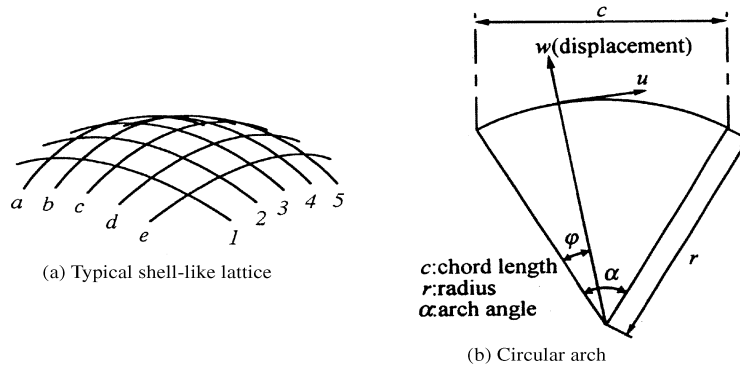‡Research Scientist

Fig. 1 Shell-like lattices and circular arch definition in monoclinic particle coordinated

(Fig. 1(a)) with circular arches and membrane are in principle of a non-conservative nature (Thompson and Stewart 1986, Jackson 1991) like a circulatory load system, because the working force is of the follower type, namely hydrostatic pressure, which works perpendicular to the deformed surface at all times. Also, disturbance forces of various types existing in a marine environment lead the structure to exhibit dynamic instabilities at a much earlier stage than could be predicted by a static stability criterion. Herein, it can be assumed that the membrane covered shell-like lattice has the role of receiving hydrostatic pressure and transferring it to the composed arches.

First of all, it is necessary to investigate the dynamic behavior of the circular arch that is the basic structural element of a shell-like lattice undergoing large deflections and small disturbances. Accordingly, the characteristics of non-periodic oscillation and the unstable state of a circular arch in the exciting forces of the circulatory load system should be grasped qualitatively. For that purpose, the governing equations for finite deformation and dynamic behavior of an arch are defined using monoclinic particle coordinates. Then, the stability region chart of the disturbed equilibrium in an excitation field is obtained numerically by analyzing the dynamic states of an arch.

From the previous study (George and Fukuchi 1993), the existence of transient regions of dynamic stability with non-periodic behavior before shifting to an unstable state has been proven. Therefore, the chaotic behaviors of a circular arch were investigated using the time intervals of motion, the power spectrum, the phase plane portraits and the *Poincare* section in the loading stage, before shifting to an unstable state. Moreover, the correlation dimension of fractal dynamics was calculated corresponding to the stochastic behaviors of a circular arch. This research clarifies that the correlation dimension related to dynamic behavior may show signs of changing from quasi-oscillatory motion to chaotic motion, and this fact indicates the possibility of making use of the correlation dimension as a stability index.

2. Dynamic equations for a circular arch under a fluctuating follower force

The equilibrium of a circular arch undergoing deformation is always prone to exhibit certain unstable behavior depending on the various disturbances that accompany changes of state or loading, due to either internal or external excitations, which are omnipresent in any physical situation.

2.1. Equilibrium equations for finite deformations

The definition of an arch, in monoclinic particle coordinates (r, φ), where r, φ are respectively the radius and the tangential angle of the arch, is shown in Fig. 1(b). The finite deformation process is assumed herein to obey the *Kirchhoff-Love* hypothesis, and the arch displacements are denoted as (u, w) depicted in Fig. 1. The general equilibrium equations of an arch (Fukuchi, Tanaka and Okada 2000) can be induced mainly from the equations for a thin shell structure (George and Fukuchi 1993) subjected to follower forces.

$$\frac{D}{r^2}\left(\frac{\partial^2 u}{\partial \varphi^2} - \frac{\partial w}{\partial \varphi} + \frac{1}{r}\frac{\partial w}{\partial \varphi}\frac{\partial^2 w}{\partial \varphi^2} + \frac{1}{r}w\frac{\partial w}{\partial \varphi}\right) = -X \tag{1}$$

$$-\frac{K}{r^4}\frac{\partial^4 w}{\partial \varphi^4} + \frac{D}{2r^4}\left[-2r^2\frac{\partial u}{\partial \varphi} - 2r^2 w + 2r\frac{\partial u}{\partial \varphi}\frac{\partial^2 w}{\partial \varphi^2} + 2r\frac{\partial u}{\partial \varphi}w + \left(\frac{\partial w}{\partial \varphi}\right)^2\frac{\partial^2 w}{\partial \varphi^2} + r\left(\frac{\partial w}{\partial \varphi}\right)^2\right.$$

$$\left. - 2rw\frac{\partial^2 w}{\partial r^2} - rw^2 + \left(\frac{\partial w}{\partial \varphi}\right)^2 w + \frac{\partial^2 w}{\partial \varphi^2}w^2 + w^3\right] = -Z \tag{2}$$

where D, K are respectively the extensional and bending stiffness; X, Z denote the tangential and normal loads of the follower type, respectively.

2.2. Dynamic stability equations for an arch subjected to small disturbances

The dynamic stability of a deformed arch on its equilibrium path under follower loads can be examined by superposing small vibration upon static deflection components. The modified governing equations of an arch, including the effect of small disturbances on the equilibrium displacement, are presented by formulating the incremental forms of Eqs. (1)~(2) and considering *d'Alembert's* principle of parametric influences due to excitation force Z_f^* as shown in the following formulas. These formulae represent stability in a disturbed state of equilibrium.

$$\rho A\frac{\partial^2 u}{\partial t^2} + E_u\frac{\partial u}{\partial t} - \frac{D}{r^2}\left(\frac{\partial^2 u^*}{\partial \varphi^2} - \frac{\partial w^*}{\partial \varphi} + \frac{1}{r}\frac{\partial w}{\partial \varphi}\frac{\partial^2 w^*}{\partial \varphi^2} + \frac{1}{r}\frac{\partial w^*}{\partial \varphi}\frac{\partial^2 w}{\partial \varphi^2} + \frac{1}{r}\frac{\partial w}{\partial \varphi}w^* + \frac{1}{r}\frac{\partial w^*}{\partial \varphi}w\right) = 0 \tag{3}$$

$$\rho A\frac{\partial^2 w}{\partial t^2} + E_w\frac{\partial w}{\partial t} + \frac{K}{r^4}\frac{\partial^4 w^*}{\partial \varphi^4} - \frac{D}{2r^4}\left[-2r^2\frac{\partial u^*}{\partial \varphi} - 2r^2 w^* + 2r\frac{\partial u^*}{\partial \varphi}\frac{\partial^2 w}{\partial \varphi^2} + 2r\frac{\partial u}{\partial \varphi}\frac{\partial^2 w^*}{\partial \varphi^2} + 2r\frac{\partial u^*}{\partial \varphi}w\right.$$

$$+ 2r\frac{\partial u}{\partial \varphi}w^* + \left(\frac{\partial w}{\partial \varphi}\right)^2\frac{\partial^2 w^*}{\partial \varphi^2} + 2\frac{\partial w}{\partial \varphi}\frac{\partial w^*}{\partial \varphi}\frac{\partial^2 w}{\partial \varphi^2} + 2r\frac{\partial w}{\partial \varphi}\frac{\partial \Delta w}{\partial \varphi} - 2rw^*\frac{\partial^2 w}{\partial \varphi^2} - 2rw\frac{\partial^2 w^*}{\partial \varphi^2}$$

$$\left. - 2rww^* + \left(\frac{\partial w}{\partial \varphi}\right)^2 w^* + 2\frac{\partial w}{\partial \varphi}\frac{\partial w^*}{\partial \varphi}w + \frac{\partial^2 w^*}{\partial \varphi^2}w^2 + 2ww^*\frac{\partial^2 w}{\partial \varphi^2} + 3w^2 w^*\right] = Z_f^* \tag{4}$$

where (*) shows the incremental quantity of displacements or forces in a momentarily disturbed state, and ρ, A are respectively the mass density and sectional area. Moreover, E_u and E_w are the damping coefficients which represent the motion frequency of arch material in both axes.

2.3. Numerical calculation method

A displacement control-type incremental load way formulated by the *Galerkin* method was employed for numerical analysis of the finite deformation and dynamic behavior of an arch. Here, we adopt the following truncated Fourier series to represent the deflection components $\{\tilde{u}, \tilde{w}\}$.

$$\tilde{u} = u + u^* = \sum_{j=1}^{m} (U_j + U_j^*)\{\phi_{1j}(j)\}, \quad \tilde{w} = w + w^* = \sum_{j=1}^{m} (W_j + W_j^*)\{\phi_{2j}(j)\} \tag{5}$$

Herein, $\phi_{1j}(j), \phi_{2j}(j)$ are the trial functions that are trigonometric series which satisfy the boundary conditions, and U_j, W_j are respectively the displacement coefficients at static state and U_j^*, W_j^* are displacement coefficients in a momentarily disturbed state. In the case of hinge edges as boundary conditions, the trial functions for displacement can be used as follows:

$$\phi_{1j}(\varphi) = \sin[(j+1)\pi \varphi/\alpha], \quad \phi_{2j}(\varphi) = \sin[j\pi \varphi/\alpha] \tag{6}$$

From several trial calculations, the number of expanding terms in a series was determined to be $m=9$. The resonances related to an outbreak of unstable state at only low frequency modes ($j=1,2$) were investigated herein. Then, an arch with a subtended angle of $60°$, as a numerical example, is assumed to be hinge edges.

Furthermore, the dynamic stability equations of an arch subjected to a sinusoidal load ($Z_f^* = Z^* \sin \omega t$) as one of the small disturbances, may be calculated numerically by using the *Runge-Kutta-Gill* method. For different pairs of values for the excitation amplitude $Z^*(N)$ and frequency ω (rad/s), the dynamic stability calculations are performed using the *Runge-Kutta-Gill* method on the initial condition of $w^*(0)=\varepsilon$, $\dot{w}^*(0)=0$ (ε: infinitesimal).

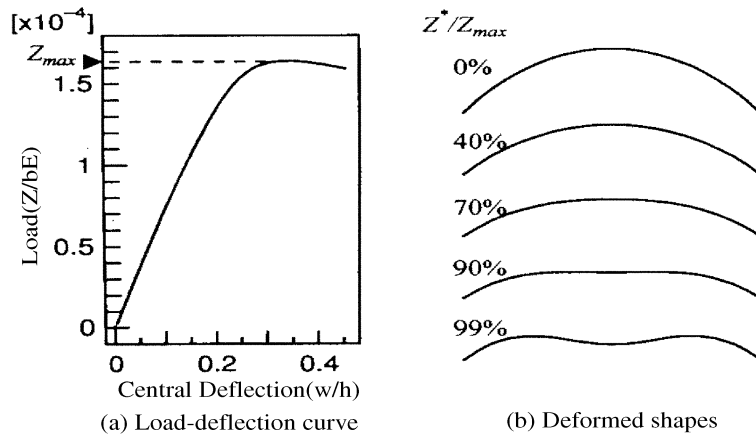(a) Load-deflection curve   (b) Deformed shapes

Fig. 2 Deformed configurations of the circular arch with loading stages

3. The dynamic behavior of the circular arch

3.1. Large deflections of a circular arch under hydrostatic follower force

The numerical results of deformed configurations for a circular arch with a subtended angle of 60^0, a sectional slender ration of 100, a Young's modulus of 1.96×10^{11} N/m^2 and a density of 7.85×10^3 kg/m^3, are shown in Fig. 2. This arch, with a square projection, was subjected to uniform hydraulic pressure acting perpendicularly to the on arch axis. The arching effect of this structure tends to decrease by forming inflection points along the arch axis.

In this case, the snapping phenomenon occurred at load Z_{cr}, that is the critical point (Z_{max}) of static stability, and the loading stage Z_x hereafter denotes x percent of the critical static load.

A previous study (George and Fukuchi 1994) clarified the existence of the stability threshold, meaning the shift point of phenomena from the heteronomous stage to the autonomous stage of self-sustained motions. It was suggested that the loading stages for design should be chosen within the stable region, and the loading stage of 70% was chosen herein for investigating dynamic behaviors during change of state from quasi-oscillatory motion to chaotic motion.

3.2. Stability regions in the excitation force field

For various sinusoidal loads (Z^* sin ωt) which work perpendicular to an arch axis, the dynamic stability of the circular arches was investigated. The state of an arch is judged to be unstable at the point when the response amplitude caused by an excitation of disturbances goes beyond one hundredth of the arch chord length within 50 periods.

The stability region on plane (ω, Z^*/Z_{max}) of disturbed equilibrium at the load stage Z_{70} is plotted in Fig. 3, the unstable border region of which makes many complex peninsular shapes (George and Fukuchi 1993), depending heavily on the amplitude and frequency of disturbance. These fractal structures (Moon 1987, Judd 1992) are mainly caused by resonance with natural frequencies. In general, the natural frequency gradually moves downward the lower positions of the excitation force
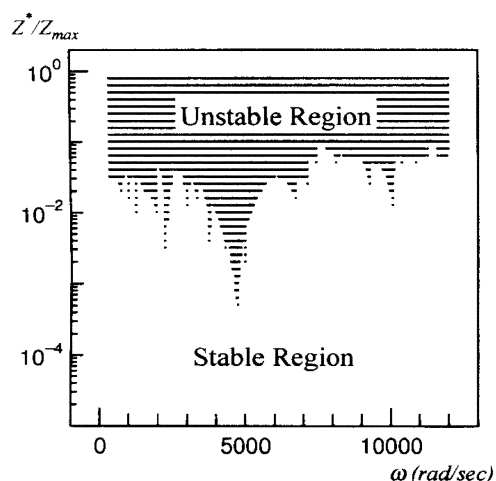

Fig. 3 Stability region of the circular arch in an excitation field [Loading stage: 70%]

field as the static load increases. The corresponding forces on a *Form-resistant structure* are changed by the variations of arch curvature, following the increase of follower force, and the arching effect tends to be especially decreased by the "M"-shaped deformation of arch configuration.

In a marine environment, there are many kinds of disturbance force with various frequencies and magnitudes. A submerged space structure receives possibly the influence of disturbances by the sound wave with a huge energy for geological survey or probing into seabed resources. As the generator of sound wave, Air-gun (5~500 Hz, 0.4~400 KJ), Water-gun (1~1000 Hz, 3~80 KJ) and Sparker (50~4000 Hz, 0.05~20 KJ) are generally used, and these frequencies are within the range of the stability region chart shown in Fig. 3.

Judging from the results of power spectrum analysis, there are three main peaks of instability in the resonance range, being nearly equal to natural frequencies ω_{Rn}=2240(rad/sec), 4710(rad/sec) and 10220(rad/sec) within the range of less than 12000 (rad/sec).

The instability regions of the neighboring ω_{R0} = 4710(rad/sec) and ω_{R1} = 2240 (rad/sec) are named respectively the *main instability region* and the *low-frequency instability region* with which the resonances of bending vibration in mode-1 and mode-3 are mostly constituent. Also, the instability region at the neighboring ω_{R2}=10220(rad/sec) is named the *high-frequency instability region* with which the coupling vibrations of in-plane motion in modes-3,1,5 and the bending motion in mode-5 are prominent.
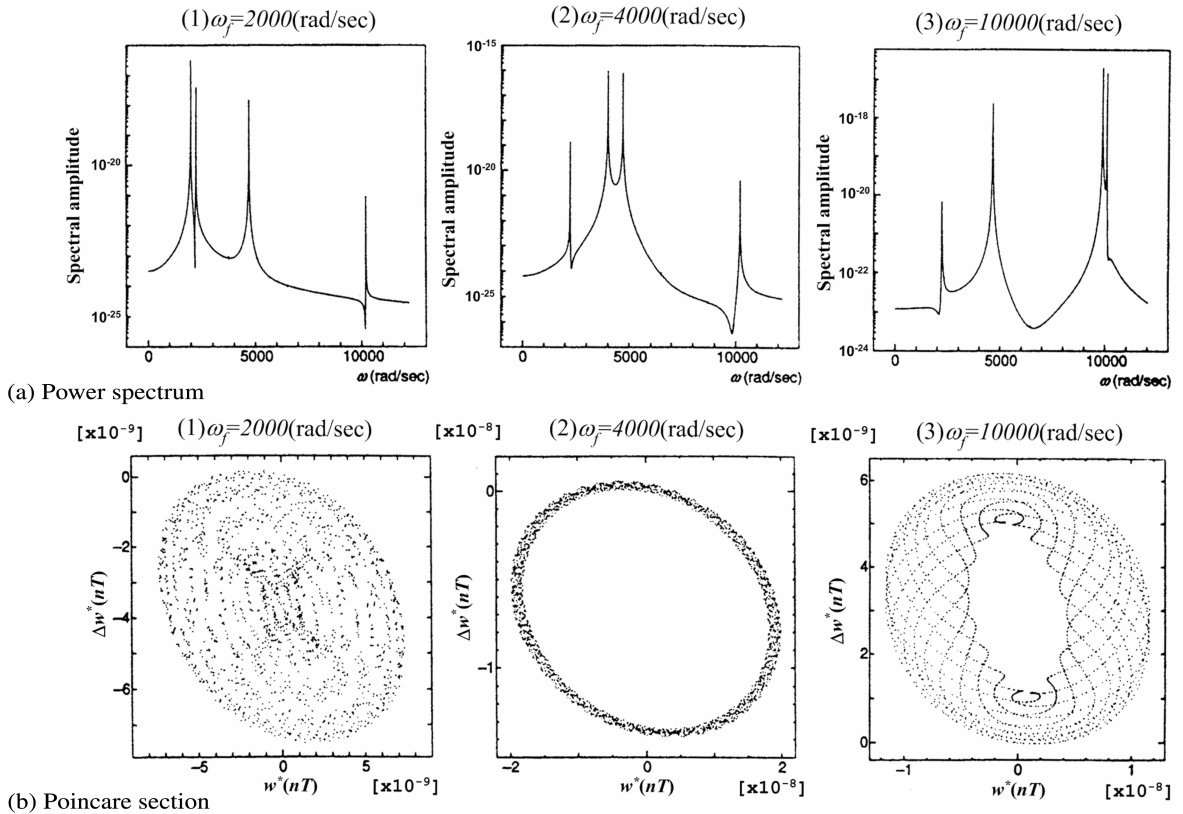

Fig. 4 Power spectra and *Poincare* sections [Loading stage: 70%, Z' = 1.00×10^{-6}]

3.3. Quasi-periodic motions corresponding to the frequency of disturbance

The response motions of a circular arch under the disturbances having the small load amplitude $Z' = 1.0 \times 10^{-6}$ and circular frequencies of the neighbor of *instability regions* were investigated using the analytical means of power spectrum and *Poincare* section. Fig. 4 is the results on the condition of {disturbance frequencies: $\omega_f = 2000$, 4000 and 10000(rad/sec)} in which the power spectra show respectively four peaks for three natural frequencies and each forced frequency. As according to the frequency of disturbance, *Poincare* sections make the change such that the ring-like aggregate points at frequency $\omega_f = 4000$(rad/sec) of the neighbor of *main instability regions* became a thin ellipse that shows to occur simple quasi-periodic motion, and the others shape a semi-geometric aggregate of discrete points that means to disappear gradually periodic property. These dynamic responses at a small load amplitude are regarded to be quasi-periodic motions in which *Poincare* section shows a elliptical aggregate of discrete points, for the composed frequencies of response motion are irrational numbers without reflexive.

3.4. Non-periodic motions in the main instability region

The response aspects of a circular arch subjected to small disturbances, having a frequency coinciding with the natural frequency $\omega_{R0} = 4710$(rad/sec) of the main instability region, were investigated with an increasing load amplitude Z'. The analytical results of the power spectrum, the response of phase
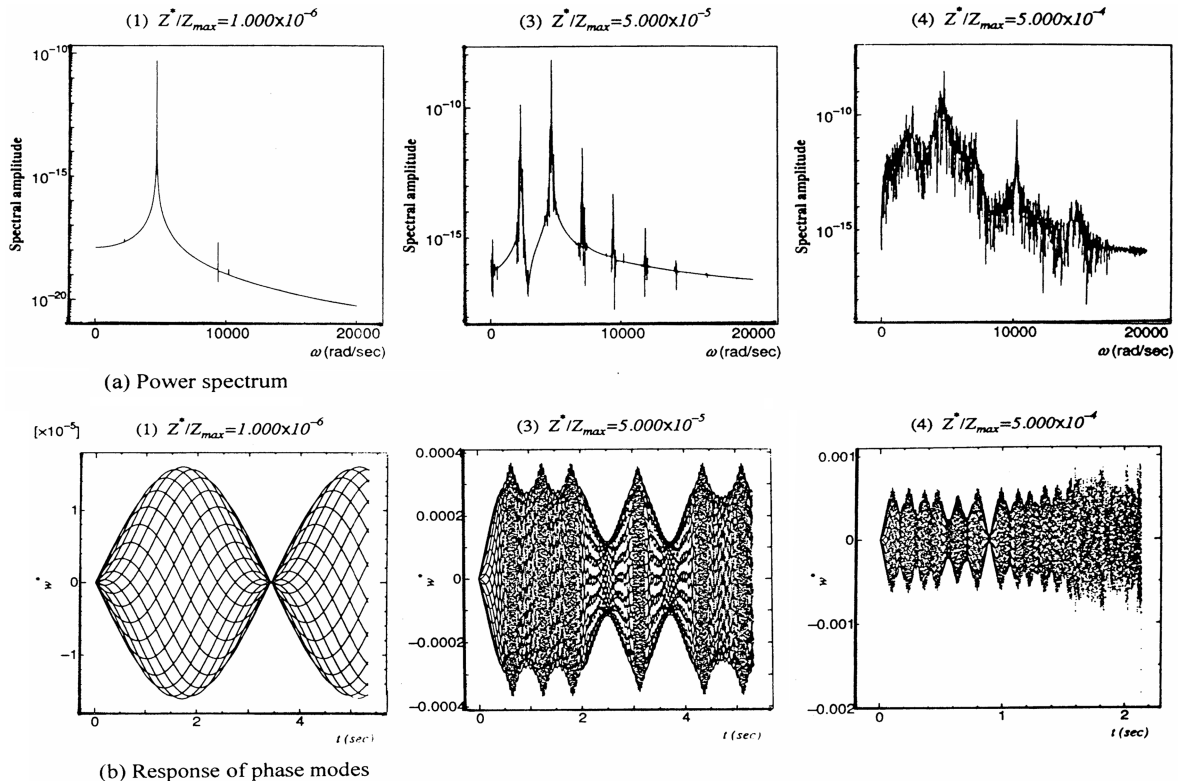

(a) Power spectrum

(b) Response of phase modes

Fig. 5 Power spectra and responses of phase modes [Loading stage: 70%, $\omega_f = 4710$ rad/sec]
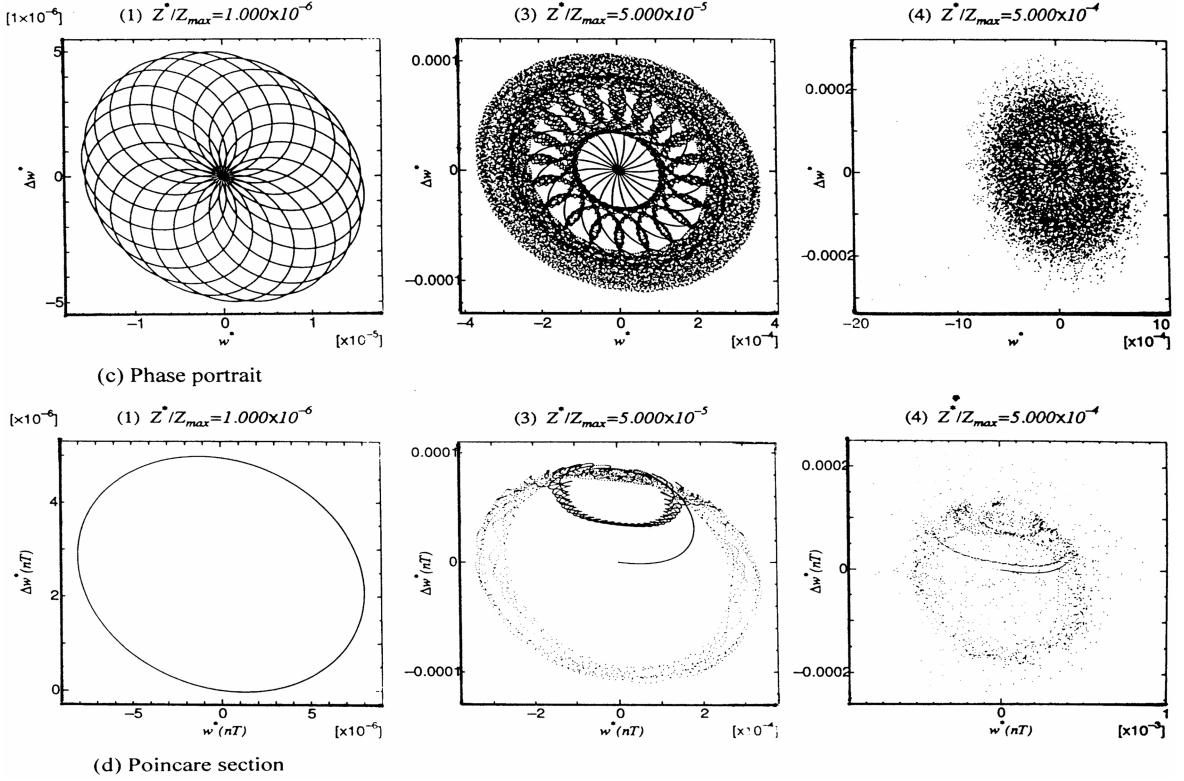
(c) Phase portrait

(d) Poincare section

Fig. 6 Phase portraits and *Poincare* sections [Loading stage: 70%, ω_f = 4710 rad/sec]

modes, the phase portrait and the *Poincare* section on the condition of {load: Z_{70}, circular frequency: ω_f = 4710(rad/sec)} are shown in Fig. 5 and Fig. 6.

When the load amplitude Z' is small, for instance Z'=1.0×10⁻⁶, there are only a few peaks corresponding to the main bending resonance, the regular bending resonance (with twice the frequency of main resonance and resonance of the coupling vibrations of in-plane motion) and the bending motion in the power spectrum chart. As the excitation amplitude increases, the number of peaks in the *low* and *high-frequency resonance regions* increase, and many peaks appear in the neighboring parts of resonance frequencies. These phenomena may be brought about by flickering motions of neighboring frequencies around the prominent motions of variations of the *Arch effect*, followed by exciting movements. Then, a large number of discrete peaks exhibit chaotic behavior within a broadband-lump of spectra, just before shifting to an unstable state.

With the increase of exciting amplitude, the response of phase modes alternates from periodic oscillation (with low frequency) to non-periodic motion, and period doubling may occur, accumulating periods and sub-critical bifurcation (Moon 1992). Moreover, the *Poincare* section is changed from a warped, single circle into a non-geometric aggregate of discrete points, because the periodic properties of dynamic motion gradually disappear, and non-oscillatory behavior become more prominent.

It was found that, going beyond a certain threshold of excitation force, a rapid expansion of non-periodic motion with large amplitudes occurs, and lastly, phase jumping may induce the outbreak of catastrophic phenomena (Thompson and Stewart 1986).

4. Judgment of stochastic motion by correlation dimensions

When the dynamic behavior of an arch is shifting from a quasi-periodic state to stochastic motion with increasing exciting forces, the following methods can be used to identify the chaotic and fractal dynamics.

4.1. Evaluation of chaotic dynamics

4.1.1. The phase plane portrait and the Poincare section

The phase plane portrait is defined as the trajectory of a set of points $(w^*, \dot{w}^*)$ which represent the angular position and velocity at times synchronous with the phase of the exciting force, and when the motion is chaotic, the trajectory tends to fill up a portion of the phase space. Also, the *Poincare* section is a synchronous point map that refers to a discrete time sampled sequence of motion data $(w^*, \dot{w}^*)$, and the phase plane portrait corresponds to the accumulation of the shifted *Poincare* sections at whole phase angles (Moon 1987, 1992).

4.1.2. Fourier power spectrum

One way to identify chaotic vibrations is to inspect the broadband response in a frequency spectrum of arch dynamics when the input is a single-frequency harmonic motion. However, in multi-degree-of-freedom motion systems, the Fourier power spectrum may have a difficult time detecting chaotic behaviors, unless one can observe changes in the spectrum as one varies parameters such as driving amplitude or frequency (Thompson and Stewart 1986).

4.2. Fractal dynamics and correlation dimensions

For recognizing chaotic behavior, the most widely used criteria are the Lyapunov exponent and the fractal dimension. These two indices are currently construed as follows: 1) Positive Lyapunov exponents denote chaotic dynamics, and 2) The fractal dimension of the trajectory in phase space denotes the existence of a strong attractor only in dissipative systems. Herein, an attractor denotes a set of points in a phase plane toward which a time interval approaches after transient states die out.

The dynamic motion response of an excited arch to some disturbances is apt to be characterized by self-similarity, that is a fractal structure, with stretching and folding of the attractor in the directions of positive *Lyapunov* exponents, such as the *Cantor* set. This characteristic can be expressed using fractal dimensions (Moon 1987, Judd 1992).

4.2.1. Embedding phase-space using single variable measurements

Since an attractor is generally the diagram of a complicated dissipative system with many state-variables, the observation of all variables tends to be difficult complicating the realization of the attractor in an objective phase space. Accordingly, it is more practical to examine the dynamic behavior at one specified point of the arch structure. Then, using the time series data of an observation point embedded into a phase space, the attractor is reconstructed and its fractal dimension is calculated. Moreover, the embedding dimension can be estimated using the saturated values of the fractal dimension.

For example, when the time series data at an observation point are given as $x_1, x_2, x_3, ..., x_t, ...$, these data are embedded into D_{em}-dimensional phase space and the state variables are reconstructed as follows;

$$X_1 = (x_1, x_{1+\tau}, \ldots\ldots, x_{1+(D_{em}-1)\tau}), \ X_2 = (x_2, x_{2+\tau}, \ldots\ldots, x_{2+(D_{em}-1)\tau}),$$

$$\ldots, \ X_n = (x_n, x_{n+\tau}, \ldots\ldots, x_{n+(D_{em}-1)\tau}), \ldots, X_t = (x_t, x_{t+\tau}, \ldots\ldots, x_{t+(D_{em}-1)\tau}) \tag{7}$$

where D_{em} denotes the embedding dimension and τ is the time interval. Then, the fractal dimension can be obtained from the reconstructed attractors.

4.2.2. The correlation dimension

In a chaotic dynamic system, the regions of phase-space may seem to be stretched, contracted or folded, and remapped onto the original space. This remapping of dissipative systems leaves gaps in the phase space, and these motion orbits tend to fill up the phase space with less than an integer of subspace. If the space is divided into $n(\varepsilon)$-cubic box with edges of size ε and the existence probability of the attractor orbit in i-th box is assumed to be p_i, a non-integer dimension of the filled subspace can be measured by the *generalized fractal dimension* D_q which is defined in the following formula.

$$D_q = \lim_{\varepsilon \to 0} \frac{1}{q-1} \frac{\log\left(\sum_{i=1}^{n(\varepsilon)} p_i^q\right)}{\log \varepsilon} \quad (-\infty < q < +\infty) \tag{8}$$

in which D_q of $q = 0$ and 1 correspond respectively to be *Capacity dimension* and the *Information dimension*. Also, D_q of $q = 2$ is called the *Correlation dimension*, which can be obtained using the accumulate distribution function between two observation points as follows;

$$D_2 = \lim_{\varepsilon \to 0} \frac{\log\left(\sum_{i=1}^{n(\varepsilon)} p_i^2\right)}{\log \varepsilon} \tag{9}$$

This formula is used herein as a sign of changing state, from quasi-oscillatory motion to chaotic motion. It is practically useful to apply the *Grassberger-Procaccia* method (Moon 1992) to calculate the formula (9).

A correlation dimension can be obtained using interrelation integration $C^{D_{em}}$ along orbital points X_i on the reconstructed attractor in the phase space of embedding dimension D_{em}.

$$C^{D_{em}}(\varepsilon) = \frac{1}{N^2} \sum_{i,j=1, i \neq j}^{N} H[\varepsilon - \|X_i - X_j\|] \tag{10}$$

where $H[\xi]$ is the *Heviside* step function defined as $H[\xi] = 1(\xi \geq 0)$ or $0(\xi < 0)$, and $\|\bullet\|$ means the *Euclid* norm. When the following equation is defined, $p_i = C_i^{D_{em}}(\varepsilon)$ is valid.

$$C_i^{D_{em}} = \frac{1}{N} \sum_{j=1}^{N} H[\varepsilon - \|X_i - X_j\|] \tag{11}$$

The term $\sum p_i^2$ in Eq. (9) can be obtained using an averaging operation, as follows:

$$\sum_{i=1}^{n(\varepsilon)} p_i^2 = \sum_{i=1}^{n(\varepsilon)} p_i C_i^{D_{em}}(\varepsilon) = \langle C_i^{D_{em}}(\varepsilon)\rangle = C^{D_{em}}(\varepsilon) \tag{12}$$

Therefore, a correlation dimension is expressed as the following formula.

$$D_2 = \lim_{\varepsilon \to 0} \frac{\log C^{D_{em}}(\varepsilon)}{\log \varepsilon} \tag{13}$$

When the following relation is valid in a suitable domain of ε, the term $d(D_{em})$ is called the *Correlation exponent*.

$$C^{D_{em}}(\varepsilon) \propto \varepsilon^{d(D_{em})} \tag{14}$$

Then, the term $\log C^{D_{em}}(\varepsilon)$ is proportional to the term $\log\varepsilon$, based on the relation obtained from the logarithm of Eq. (14). According to the dimension D_{em} of the reconstructed phase space, when D_{em} is smaller than the dimension of actual attractors, the term $d(D_{em})$ approaches D_2 for the reconstructed phase space covered with attractors.
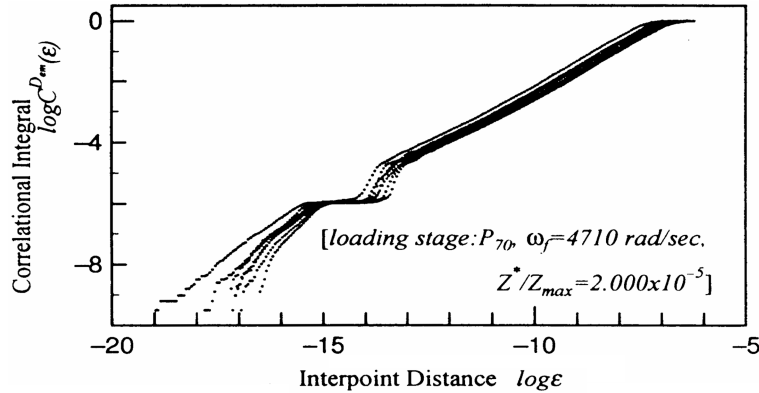

Fig. 7 The values of correlation integral and distributions of inter-point distances for embedding dimensions 2 to 8
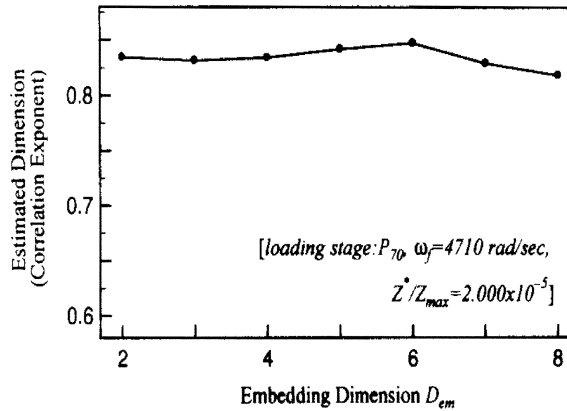

Fig. 8 Estimating correlation exponents for embedding dimensions 2 to 8

4.3. Attractors and correlation exponents of dynamic behaviors

Using the results of dynamic analysis of the circular arch, the relation between the *Correlation integral* $\log C^{D_{em}}(\varepsilon)$ and distributions of inter-point distances for the embedding dimensions: D_{em}=2 to 8 are obtained using the *Grassberger-Procaccia* method (Moon 1992) as shown in Fig. 7. A gradient of the correlation integral in this figure denotes *Correlation exponent*, and Fig. 8 shows the relation between the estimated correlation exponents and the embedding dimensions. This relationship indicates that the correlation exponent is almost converged over D_{em}=2 similar to other numerical examples. Consequently, the dynamic characteristics of attractors can be calculated using D_{em}=3.

As the embedding dimension increases, the reconstructed attractors (shown in Fig. 9) exhibit very similar dynamic aspects, regardless of D_{em}. Accordingly, the dynamic characteristics of attractors can be grasped in a two-dimensional phase plane. Further, in the case of D_{em}=4, the projection of a 4-dimensional hyper-cube reflects that of a 3-dimensional space.
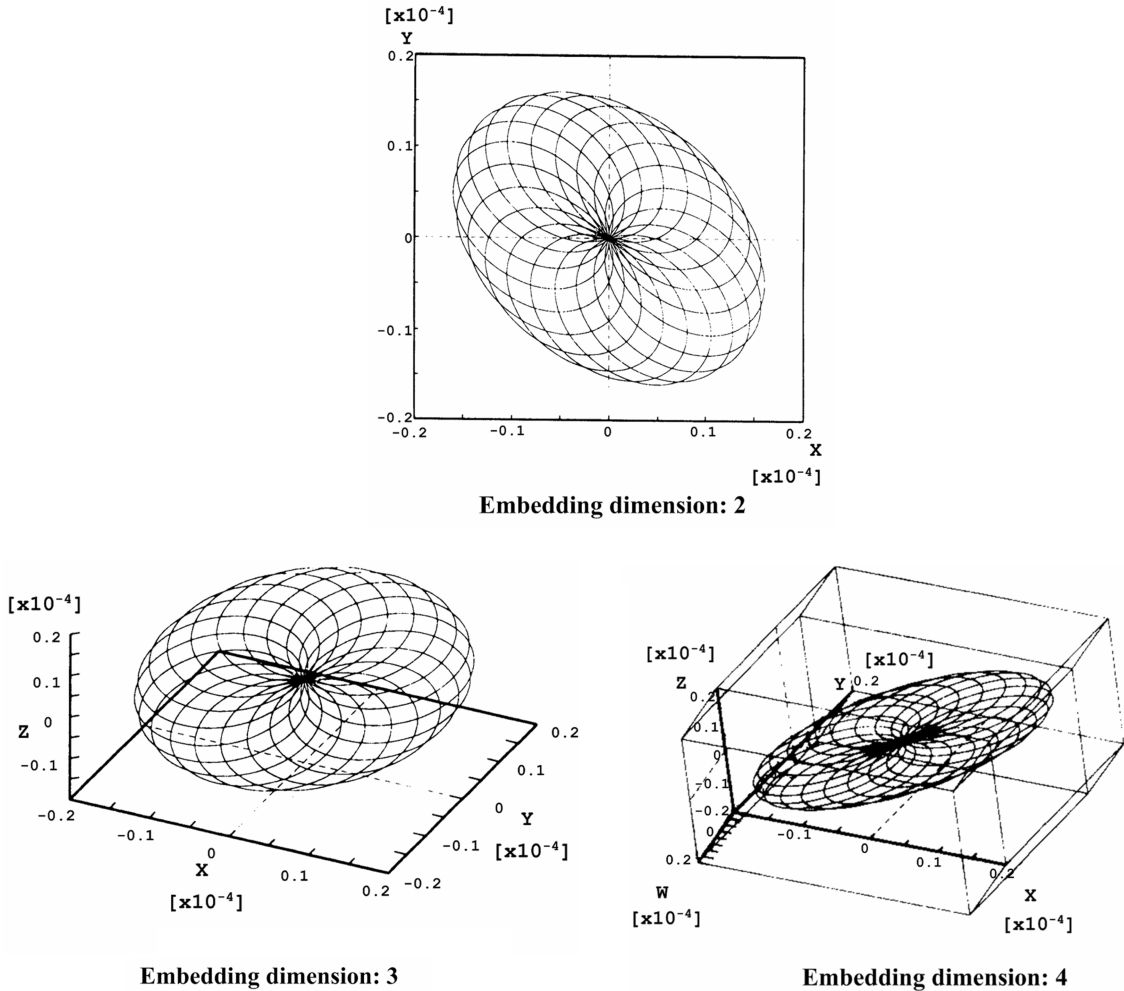

Embedding dimension: 2

Embedding dimension: 3

Embedding dimension: 4

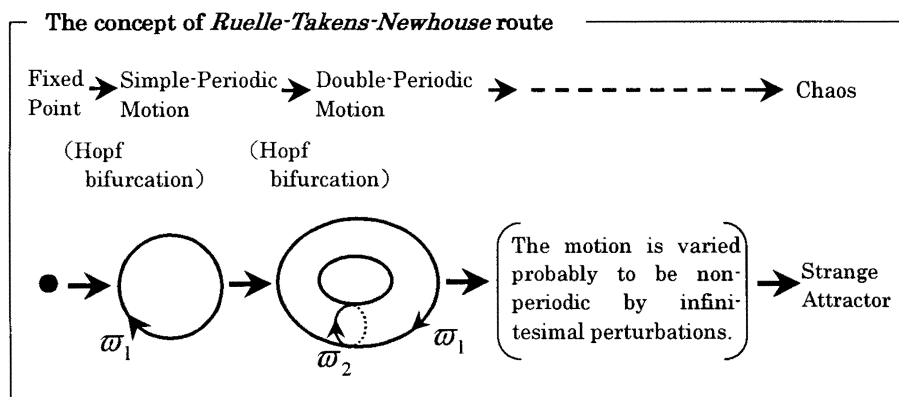Fig. 9 Reconstructed attractors [Z=1.00×10^{-6}]

Fig. 10 A concept of *Ruelle-Takens-Newhouse* route

5. A scenario of chaotic behaviors and fractal dynamics

5.1. The change from quasi-periodic oscillation to chaotic motion

When a forced frequency of disturbances nearly coincides with a natural frequency, the process of dynamic behaviors toward chaotic motion is as follows;

1) The quasi-periodic oscillation associated with a forced frequency which exhibits a hauling phenomenon, occurs because of the difference between the two frequencies.

2) As the excitation amplitude Z' increases, an oscillation with many spectral peaks breaks out, because of combined oscillations and flickering motions around the distinguished motions.

3) Then, chaotic behavior appears with broadband-lump of discrete spectral peaks, and the non-periodic motions shift to an unstable state.

This phenomenon, in which a single periodic motion develops into double periodic motion by *Hopf*-bifurcation and finally shifts to chaotic motion, is called the *Ruelle-Takens-Newhouse* scenario (shown conceptually in Fig. 10). This scenario seems to be the same as Benard's heat conduction (Martin and Leber 1984) and the dynamic behavior of a nonlinear vibrator (Buskirk and Fefferis 1985), but it is different from the *Feigenbaum* scenario, in which the chaotic state is caused by period-bifurcations and the final state becomes unstable by *flip*-bifurcation (like the *Duffing* dynamic system) (Buskirk and Jeffries 1985, Libchaber and Maurer 1982).

5.2. The correlation dimensions of the process toward chaotic motion

While the load amplitude Z' was gradually increased, the correlation dimensions in the case of a circular arch subjected to small disturbances which have a frequency coinciding with the natural frequency $\omega_{R0} = 4710(\text{rad/sec})$ (as in paragraph 4.4) were calculated. Fig. 11 is respectively the variation of power spectra and the estimated correlation dimension D_2 as the excitation amplitudies increases. Considering these results combined with those of Fig. 5 and Fig. 6, the varying aspects of the correlation dimension can be found as follows:

1) When the excitation amplitude Z' is below 2×10^{-6}, the arch is in a quasi-periodic state of oscillation, with few spectral peaks corresponding to the bending resonances, and the estimated correlation
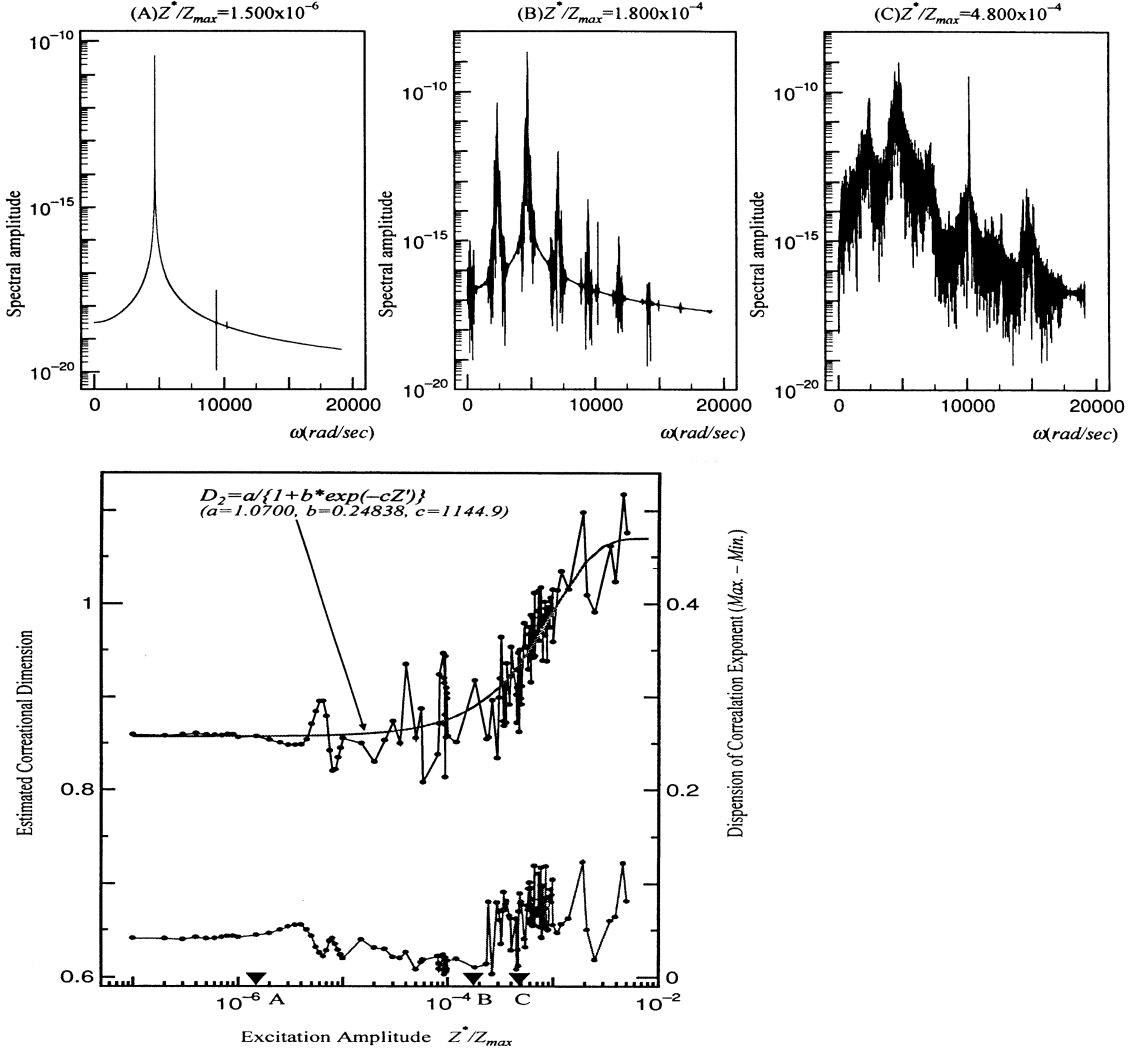
Fig. 11 Variation of power spectra and estimated correlation dimensions D_2 as enlarging excitation amplitudes

dimension is almost constant at about 0.86 and the correlation exponent disperses within about 0.03.

2) As the excitation amplitude increases, the correlation dimension fluctuates deeply because of flickering motions with neighboring frequencies around the distinguished motions according to the variation of *Form-resistance* by excitation movements. But the dynamic motion depends considerably upon prominent spectral peaks, and the dispersions of the correlation exponent remain nearly constant.

3) When Z' is over 3×10^{-4}, a large number of discrete peaks with a broadband-lump of spectra appear, and the motion shifts to chaotic oscillation. The estimated correlation dimension fluctuates wildly because of the uneven correlation exponent associated with stochastic motions. As the exciting amplitude increases, the non-periodic properties also increase, and the correlation dimension finally reaches a maturity of disturbance.

Consequently, when disturbances are fully-developed and the fractal aspect converges upon the ultimate condition, the dynamic motion is denoted as be chaotic behavior. Hence, the variation of the correlation dimension can be generally expressed using a logistic curve like as $D_2=a/\{1+b\cdot\exp(-c\cdot Z')\}$.

6. Conclusions

The dynamic behaviors of a circular arch under hydraulic follower forces with small disturbances were investigated by using the time interval of motion, the power spectrum, the phase plane portraits and the *Poincare* section in the resonance region. According to these results, the change of state from quasi-oscillatory motion to chaotic motion and the correlation dimension in fractal dynamics of a circular arch can be clarified with the following items.

1) In the case that a forced frequency of disturbances nearly coincides with a natural frequency, the process toward chaotic motion is based on the *Ruelle-Takens-Newhouse* scenario in which a single periodic motion develops into double periodic motion by *Hopf*-bifurcation and finally shifts to chaotic motion.

2) As the excitation amplitude increases, a large number of discrete peaks with a broadband-lump of spectra appear, and the motion shifts to chaotic oscillation. The correlation dimension fluctuates wildly because of the uneven correlation exponent associated with stochastic motions, and the correlation dimension finally reaches a maturity of disturbance.

References

Buskirk, R. V. and Jeffries, C. (1985), "Observation of chaotic dynamics of coupled nonlinear oscillations", *Physics Review*; **A31**, 3332-3357.

Fukuchi, N., Tanaka, T. and Okada, K. (2000), "A characteristic analysis on dynamic stability of shell-like lattice structures subjected to follower forces", *Advances in Computational Engineering and Sciences*; **2**, 1816-1821.

George, T. and Fukuchi, N. (1993), "Dynamic instability analysis of thin shell structures subjected to follower forces, (4th Report) quantitative stability of disturbed", *J. of the Society of Naval Architects of Japan*; **174**, 787-796.

George, T. and Fukuchi, N. (1994), "Dynamic instability analysis of thin shell structures subjected to follower forces, (5th Report) disturbance threshold curves of dynamic stability", *J. of the Society of Naval Architects of Japan*; **175**, 337-348.

Jackson, E. A. (1991), *Perspectives of Nonlinear Dynamics 1*, Cambridge University Press.

Judd, K. (1992), "An improved estimator of dimension and some comments on providing confidence intervals", *Physica*; **D56**, 216-228.

Libchaber, A. and Maurer, J. (1982), "A Rayleigh benard experiment: Helium in a small box", *Nonlinear Phenomena at Phase Transitions and Instabilities*; 259-286.

Martin, S., Leber, H. and Martinsen, W. (1984), "Oscillatory and chaotic states of the electrical conduction in barium sodium niobate crystals", *Physics Review*; Lett. **53**, 303-306.

Moon, F. C. (1987), *Chaotic Vibrations*, John Wiley and Sons.

Moon, F. C. (1992), *Chaotic and Fractal Dynamics*, John Wiley and Son.

Thompson, J. M. T. and Stewart, H. B. (1986), *Nonlinear Dynamics and Chaos*, John Wiley and Sons.

CC